ELSEVIER

The Managua Graben and Las Sierras-Masaya volcanic complex (Nicaragua); pull-apart localization by an intrusive complex: results from analogue modeling

Guillaume Girard*, Benjamin van Wyk de Vries

Laboratoire Magmas et Volcans, Observatoire de Physique du Globe de Clermont-Ferrand, Université Blaise-Pascal-CNRS, UMR 6524, 5, rue Kessler, 63038 Clermont-Ferrand, France

Abstract

There is a well-documented association between pull-apart basins in strike-slip zones and large volcanic caldera complexes. Las Sierras-Masaya volcanic complex, Nicaragua, is a large basaltic lava and ignimbrite shield with nested calderas. The widest caldera is partly underlain by a large and dense intrusive complex, evidenced by a positive gravity anomaly. The Las Sierras Caldera, relating to this cumulate complex, is less than 30,000 years old and is probably still hot and ductile. The inner Masaya Caldera hosts an active magmatic system. The volcanic complex is in a dextral transtensional tectonic context of the Nicaraguan Depression. The highly active Managua Graben is on the northern part of the volcano. We speculate that the graben and volcano are linked tectonically, with the graben initiating in response of a regional stress field modified around the dense, ductile intrusive complex. Previous field work and reappraisal of structures with digital elevation model morphological analysis show that the volcano is surrounded by a rhombic fault pattern that may form a nascent pull-apart basin. We have done scaled analogue models to test the effect of intrusion density and rheology anomalies on strike-slip fault geometries. The models show that intrusion density variations alone do not significantly change fault patterns. In contrast, ductile rocks (silicone in the models as analogue for hot mafic intrusive rocks) markedly alter strike-slip fault patterns. In transtension the presence of a ductile intrusion causes the formation of a pull-apart, while in pure strike-slip or transpression, uplift and thrusting is generated. Pull-apart and uplift structures are rhomb-shaped even when the ductile inclusion is circular. We conclude that a pull-apart is developing at Las Sierras-Masaya volcanic complex in response to the transtensive regional deformation regime and the dense, ductile

---

* Corresponding author. Present address: Earth and Planetary Sciences, McGill University, 3450 University Street, Montréal, Québec, Canada H3A 2A7. Tel.: +1 514 398 5391; fax: +1 514 398 4680.

E-mail addresses: ggirard@eps.mcgill.ca (G. Girard), b.vanwyk@opgc.univ-bpclermont.fr (B. van Wyk de Vries).

intrusive complex. We suggest that the volcano and graben are one dynamic system and should be monitored as one entity.

1. Introduction

It is now widely accepted that volcano loading may partly control fault patterns. For example, loading by large shield volcanic complexes can alter regional fault directions (van Wyk de Vries and Merle, 1998). This phenomenon has been well reproduced in laboratory for a range of tectonic regimes (van Wyk de Vries and Merle, 1996, 1998; Branquet and van Wyk de Vries, 2001; Lavallée et al., 2004). Volcanoes and large intrusive bodies may also influence faulting on other planets (e.g. Cyr and Melosh, 1993; Watters and Janes, 1995). Exhumed intrusive bodies at some calderas are associated with sinking structures that may be due to density and rheological weaknesses (Walker, 1988; Glazner and Miller, 1997).

Las Sierras-Masaya volcanic complex, one of the largest volcanoes of the Pacific coast of Nicaragua, is underlain by a large and dense magmatic intrusion (Metaxian, 1994). The Managua Graben, one of the most active tectonic structures of Central America lies on the north flanks of the volcano. The volcano and graben have formed over the same time period and we suggest that the structural evolution of the two may be linked through an interplay between regional and volcano tectonic processes. At present, the origin of the recent faulting in the whole area is being vigorously debated. The debate is about the comparative effects of Caribbean Plate and Pacific Plate motions and the local effect of volcano-tectonics (Burkart and Self, 1985; van Wyk de Vries, 1993; van Wyk de Vries and Merle, 1996, 1998; La Femina et al., 2002). To contribute to the debate we propose a volcano-tectonic origin for the Managua Graben. We present a digital elevation model (DEM) morphostructural-structural analysis, supported by previous field observations of the Las Sierras-Masaya volcanic complex and the Managua Graben. We model the effect of the dense, ductile intrusive body with analogue models and conclude that the formation of

the graben is probably linked to the presence of the intrusion beneath Masaya Caldera.

2. Las Sierras-Masaya and the tectonics of Nicaragua

2.1. Tectonic context of western Nicaragua

Las Sierras-Masaya volcanic complex is related to subduction of the Cocos Plate beneath the Caribbean plate. Subduction beneath Central America is slightly oblique, from 0 to 15°, and movement on the northern boundary of the Carribean Plate is strike-slip (the Montagua-Cayman fault). These obliquities result in an anti-clockwise rotation of the crustal blocks (Burkart and Self, 1985; Manton, 1987; La Femina et al., 2002). Owing to this rotation, and/or as a consequence of the oblique subduction, the Pacific margin of Central America in under a dextral strike-slip tectonic regime and small amounts of orthogonal extension. The average velocity of this lateral motion is about 14 mm/year (DeMets, 2001). Some dextral strike-slip faults are well developed along the margin, such as Jalpatagua fault in Guatemala (Burkart and Self, 1985), but there is no clear evidence of strike-slip trench-parallel faulting in Nicaragua. However, there is a large depression, the Nicaraguan Depression (Fig. 1). Almost all the Quaternary volcanoes of Nicaragua, including Las Sierras-Masaya, lie within this structure (McBirney and Williams, 1965).

Initially interpreted as a graben (McBirney and Williams, 1964, 1965), the Nicaraguan Depression was later redefined by van Wyk de Vries (1993) as a low-lying area bounded by a Tertiary volcanic Highland region and a Pliocene formed coastal fold belt. Faulting in the Nicaraguan Depression principally consists of perpendicular northeast-striking left-lateral faults possibly defining bookshelf faulting (La
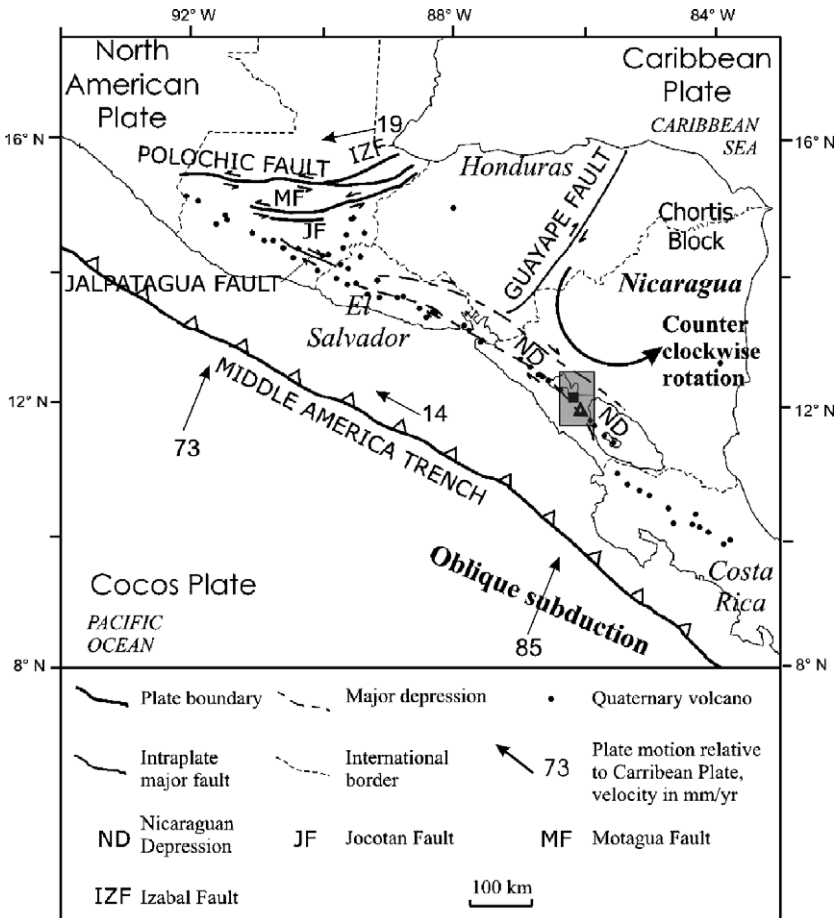
Fig. 1. Map of Central America, showing relative plate motions. The gray rectangle is our investigation area (Managua Graben); the black square in it represents Managua City and the triangle Las Sierras-Masaya volcanic complex. Motion on Guayape fault is from Gordon and Muehlberger (1994), major faults and rotation are compiled from Burkart and Self (1985), plate motion and velocities are from DeMets (2001) and are expressed relative to the Caribbean Plate. Map modified from DeMets (2001).

Femina et al., 2002), instead of northwest-striking right-lateral faults. This fault pattern could be the immature expression of a dextral strike-slip tectonic regime where R' faults are favored, as suggested by the analogue experiments of Freund (1974). There may be an influence from earlier-formed northeast-striking faults north of the Nicaraguan Depression (Manton, 1987; Weinberg, 1992), and also volcano-tectonic effects (van Wyk de Vries and Borgia, 1996; van Wyk de Vries and Merle, 1998). A right-lateral strike-slip stress pattern does exist at the scale of the Depression, to fit with regional plate tectonics, even if its surface expression and interpretation is still controversial.

2.2. Las Sierras-Masaya volcanic complex

Las Sierras-Masaya volcanic complex is the largest Quaternary volcano of Nicaragua. It consists of Las Sierras, a basaltic ignimbrite shield that surrounds a complex system of calderas, of which Masaya Caldera is the most recent one (Fig. 2; van Wyk de Vries, 1993; Šebesta, 1997). Masaya Caldera hosts Masaya Volcano, one of the most active of Nicaragua, well-known for its intense magmatic degassing. Studies have focused on the origin of Masaya Caldera from basaltic plinian eruptions (e.g.: McBirney, 1956; Bice, 1980; Williams, 1983) and on the present activity of Masaya
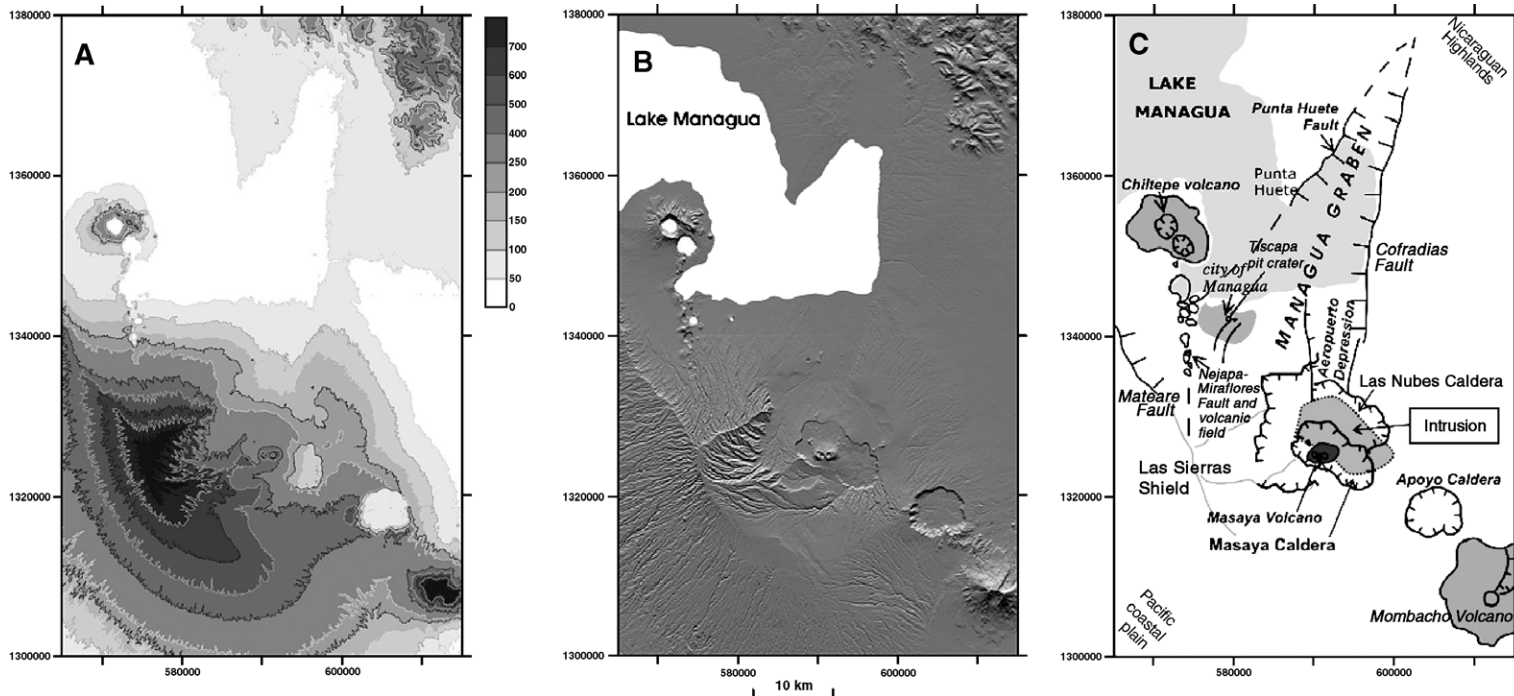
Fig. 2. Map of the studied area. (A) Topography of the studied area, with contours every 50 m. (B) 30m resolution DEM shaded relief image. (C) General structural maps, made from the DEM. The Managua Graben is the depression bounded by Punta Huete, Nejapa-Miraflores/Mateare and Cofradías faults and unclearly bounded by Masaya Caldera and Las Sierras shield at South. Note that the city of Managua lies very close to Nejapa-Miraflores and Masaya volcanoes and at the center of the Managua Graben.

Volcano (e.g. Rymer et al., 1998; Horrocks et al., 1999; Burton et al., 2000; Delmelle et al., 2002). The internal structure of the volcano has also been studied by Metaxian (1994), who, following a preliminary study by Connor and Williams (1989), used gravity data to show that there was a 6 km thick, 3–9 km deep and 10–15 km in diameter underlying intrusion, 600 kg/m^3 denser than the surrounding rocks. Slightly reduced seismic velocity data indicates that although the intrusion may not contain any melt, but is still probably hot enough to be ductile (Metaxian, 1994).

The Las Sierras-Masaya volcanic complex initiated in the early Quaternary, or even Pliocene (McBirney and Williams, 1965). The first deposits are dacitic ignimbrites found on the north–east side of the Nicaraguan Depression (van Wyk de Vries, 1993). These are covered by a group of ignimbrites and associated lahars of basaltic composition that form the main relief of Las Sierras shield (Fig. 2). This shield was cut by the Mateare Fault to the northwest, while a caldera complex formed to the southeast (Fig. 1). The exact limits of the early calderas are not clear (Šebesta, 1997), but at 30,000 BP a large basaltic
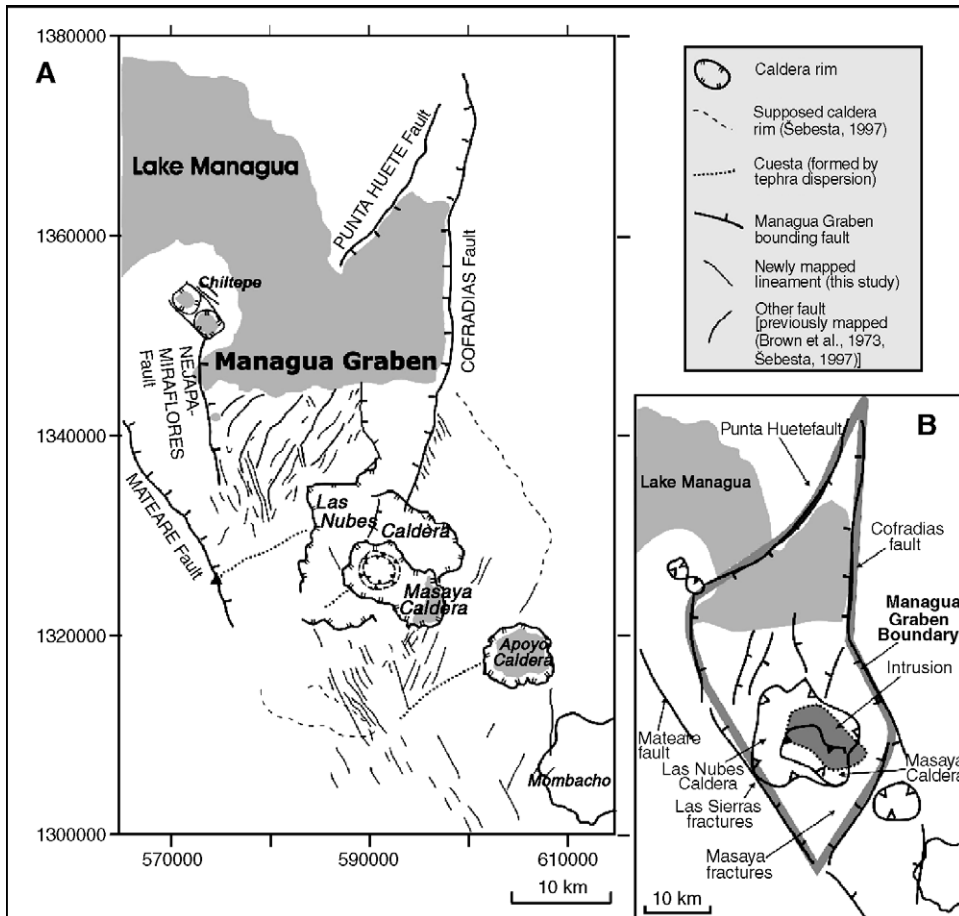

Fig. 3. (A) Structural map made from the DEM that shows, in addition to the clear Managua Graben bounding faults and the system of calderas (Šebesta, 1997), three families of faults (1) NNE-striking faults south of Masaya Caldera extending Cofradías fault, (2) numerous NE-striking faults between Masaya Caldera and Lake Managua, probably associated with the faults active during the recent earthquakes (Brown et al., 1973) and principally, (3) NNW-striking faults along the western side of the graben, extending Nejapa-Miraflores and Mateare faults. Those newly mapped structures draw a rhombic basin around Las Sierras-Masaya, allowing us to consider the Managua Graben as a pull-apart. (B) Schematic reconstruction of the main features of the Managua Graben and Las Sierras-Masaya volcanic complex.

ignimbrite was erupted and a large caldera was formed, that is still a clear morpho-structural feature (Bice, 1980). This caldera is called Las Nubes by Šebesta (1997) and Las Sierras by van Wyk de Vries (1993). The ignimbrite deposit is found in the Managua region, where is it cut extensively by the Managua Graben faults. Some faults, such as the Cofradías join the caldera structure and may have moved during caldera formation (Fig. 2). The Cofradías fault and others in the graben have been active over historical times (Brown et al., 1973). After the formation of the Las Sierras Caldera, basalt lavas formed a shield, Masaya Volcano. This was partially destroyed by a group of plinian and ignimbrite-forming eruptions culminating in the Masaya surge at about 4000 BP (Bice, 1980; Williams, 1983). During this time (at about 20,000 years BP) the Apoyo Caldera (Fig. 2) formed during a major silicic ignimbrite eruption (Bice, 1980). The resulting caldera has been partially filled by a new basaltic lava shield that started to overflow into the Managua Graben in 1772 (McBirney and Williams, 1965).

As the ignimbrite that formed the Las Sierras Caldera blanketed the topography, the present faulted and eroded surface dates from less than 30,000 years, except for the larger features such as the Mateare Fault and the Nejapa-Miraflores fault (Figs. 2 and 3).

3. Managua Graben

The Managua Graben is the most active tectonic structure of the Nicaraguan Depression. The main faults are orientated north-northeast and north (Fig. 2). Damaging shallow earthquakes have occurred in 1931, 1968 and 1972 (Brown et al., 1973). While called a graben, it is only partially bounded by clearly visible normal fault scarps (Fig. 2). The Punta Huete Fault, on its northwestern side and the Cofradías Fault on the eastern side are the most evident ones, with scarps that reach more than 100 m high (Šebesta, 1997). The westernmost side of the basin is delimited by the Nejapa-Miraflores Fault (Fig. 2), along which lies an alignment of basaltic cinder cones and pit craters (Walker, 1984), and the Mateare Fault, the largest fault scarp in Nicaragua (van Wyk de Vries, 1993; Šebesta, 1997). The Graben's southern boundary is the Las Sierras-Masaya volcanic complex. The graben has

been interpreted as a pull-apart basin (Šebesta, 1997). Two main fault zones have been mapped in the graben (Fig. 2): (1) Aeropuerto Depression, a small graben bounded by Aeropuerto and Cofradías faults that extends south into the Las Sierra Caldera, and (2) a left-lateral strike-slip fault zone is located around Managua City (Šebesta, 1997). This zone is where recent seismicity is concentrated (Brown et al., 1973) and may be an extension of Punta Huete fault under Lake Managua (Fig. 2). The rest of the graben is occupied by Las Sierras-Masaya and Lake Managua, in which few faults have been mapped, but where seismic evidence indicates active faulting (Brown et al., 1973).

Using the previous field work (e.g. van Wyk de Vries, 1993; Šebesta, 1997) and a 30 m resolution Digital Elevation Model, a detailed morpho-structural and lineament has been done. The main known faults of the Managua Graben are well represented on the DEM (Fig. 2B), as well as erosion and depositional features. As there is a good correlation between the DEM features and previously mapped structures, so we could confidently extend the analysis to the whole of the Las Sierras-Masaya volcanic complex. Some lineaments are scarps with clear fault-related origin, others are surface features that may be faults. Some gully features may contain faults, as they hold consistent strikes, or are smooth curved features. Verification in the field of such features is difficult, as the gullies are typically sediment-filled, and structural features are masked. Trench digging in Managua on such features has usually exposed fractured rock and off-sets.

On the DEM illustrated morphology (Fig. 2B), we observed that there are numerous faults, lineaments and possible fault controlled erosion around Las Sierras-Masaya, defining three groups (Fig. 3A). (1) Some NNE-striking faults south of Masaya Caldera may be a southward extension of Cofradías fault, while (2) numerous northeast-striking faults between Masaya Caldera and Lake Managua are probably associated with the faults active during the recent earthquakes (Brown et al., 1973). The most numerous are (3) north-northwest-striking faults along the western side of the graben. They can be considered a southward extension of Nejapa-Miraflores and Mateare Fault trends.

The Aeropuerto Depression changes as it approaches Las Sierras-Masaya and the bounding normal

faults evolve into a family of smaller faults that have fresher and sharper topography. This suggests that faulting is younger, or more active towards the volcanic complex center. This change in the surface expression of the faulting can be the consequence of one basement fault cutting recently deposited material and bifurcating. Otherwise it could be a consequence of the volcano load that causes fault densification (van Wyk de Vries and Merle, 1996). There is a set of faults between Masaya Volcano and Apoyo Volcano that closes the southern border of the Managua Graben, to complete a rhomb-shape (~50 km long in NNW direction and 20 km wide). There is a northern extension that progressively narrows to evolve into a triangular graben between the Cofradías Fault and the Punta Huete Fault (Fig. 3). Given that the faults near Managua City and the Cofradías Fault have a strong sinistral strike-slip component (Brown et al., 1973; van Wyk de Vries, 1993), and that the regional trend is dextral, the Managua Graben has been interpreted as a pull-apart basin (Šebesta, 1997). Our interpretation of its rhombic shape reinforces that interpretation. The graben morphology (50×20 km) gives an aspect ratio of 2.5, close to the aspect ratio of 3, characteristic of most pull-apart basins (Aydin and Nur, 1982).

These above observations show a spatial link between the graben and the Las Sierras-Masaya volcanic complex. We also know that the two structures are contemporaneous: both began to form at about 1 Ma ago, and both are still active today (Weinberg, 1992; van Wyk de Vries, 1993; Šebesta, 1997). We suggest that the volcanic complex, and most specifically the dense pluton, have localized faulting and generated the pull-apart through density and rheological contrasts. To test this we ran a series of analogue models representing the magmatic system in the dextral strike-slip tectonic environment that characterizes the Nicaraguan Depression.

4. Analogue modeling

4.1. Experimental setup

The models represent Las Sierras-Masaya intrusive complex in the strike-slip tectonic context of the Nicaraguan Depression. To model this environment, we used sand and silicone putty, with an upper brittle layer made of sand representing the brittle upper crust and an underlying ductile layer made of silicone equivalent to the more ductile lower crust. The boundaries of the models were constrained by brittle sand so as to avoid any lateral spreading. We used a transparent silicone Silbione 70 009; produced by Rhodia), the quoted viscosity of this silicone is approximately 10^5 Pa s, at experimental conditions (room temperature). We constantly checked the viscosity of the silicone on a rotational viscometer (see scaling). Displacements were applied to one half of the model, by a thin basal sheet placed just below the base of the model and linked to a step motor (Fig. 4). The moving
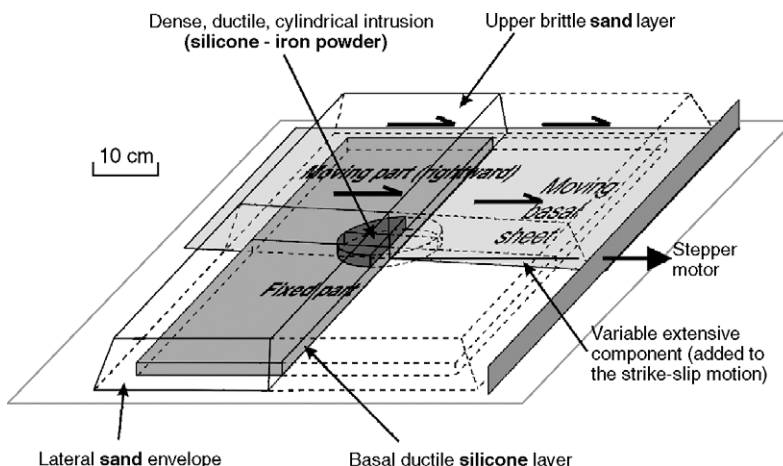

Fig. 4. Experimental setup.

part represents the northern side of the Nicaraguan Depression, which shows a dextral movement resulting from Chortís block rotation (Burkart and Self, 1985; Manton, 1987; Gordon and Muehlberger, 1994). The immobile second part represented the Pacific coastal plain southwest of the Depression. Movements are, of course, relative, so either side can be regarded as fixed, or in movement, or both can be considered to be mobile (van Wyk de Vries and Merle, 1998; Lagmay et al., 2000). There was a small deviation from pure strike-slip motion on the plate, which amounted to an error of about +/− of less than 1°.

In most cases the intrusion was placed at the center of the model, lying directly on the silicone layer. In a few experiments it was offset to verify that the structures formed above the intrusion were really the result of the intrusion rather than a structure that would appear at the centre of the model. The intrusion was made of a mixture of silicone and iron powder, silicone being used to make it ductile, and iron powder to increase its density. It was then covered with a layer of sand

(Fig. 4), while respecting geometric similarity of a brittle upper crust thickness (Tables 1–3).

4.2. Scaling

Choice of the analogue materials was made following previous experiments modeling tectonics in the crust and volcanic systems (e.g. Tron and Brun, 1991; McClay and Dooley, 1995; van Wyk de Vries and Merle, 1996, 1998; see also Cobbold and Castro, 1999, for a review). For both economical and practical reasons, silicone was recycled from previous experiments and thus initially contained a small fraction of sand. The effect was increase in viscosity of about one order of magnitude that was monitored. The overall dimensions of the models were ~70×50 cm on average, for practical reasons. Heights were fixed by respecting geometric similarity (constant aspect ratio between models and nature). The length scale was determined using the depth of the brittle crust (assumed to be roughly 10 km) compared with the thickness of brittle sand in the model (3.5 cm).

Table 1
Values of physical parameters in nature and experiments, and their experiment/nature ratio

Symbol	Definition	Units (S.I.)	Nature	Value Models	Ratio model/nature	
h_u	Height of upper layer	m	10^{4a}	$3.5×10^{-2}$	h_u*	$3.5×10^{-6}$
h_i	Height of lower layer[b]	m	$10^3–10^{4b}$	$1.5×10^{-2b}$	h_1*	10^{-6}
h_i	Height of intrusion	m	$6×10^{3a}$	$2.5×10^{-2}$	h_i*	$4×10^{-6}$
r_I	Radius of intrusion	m	$7.5×10^{3a}$	$3.7×10^{-2}$	r_i*	$5×10^{-6}$
ρ_u	Density of upper layer	kg m^{-3}	2400^c	1400	ρ_u*	0.6
ρ_1	Density of lower layer	kg m^{-3}	2800	1550 (1080)	ρ_1*	0.55 (0.4)
ρ_I	Density of intrusion	kg m^{-3}	3000^a	1610 [2000]	ρ_1*	0.55 [0.67]
C_u	Cohesion of upper layer	Pa	$10^7–10^8$	$10–10^{2d}$	C_u*	10^{-6}
$[C_i]$	[Cohesion of intrusion]	Pa	$10^7–10^8$	$[10–10^2]$	$[C_1]*$	$[10^{-6}]$
Φ	Angle of internal friction		30°	30°	$\Phi*$	1
η_1	Viscosity of lower layer	Pa s	$10^{20}–10^{21e}$	$~10^6$ ($6×10^4$)	η_1*	$10^{-14}–10^{-15}$
η_i	Viscosity of intrusion	Pa s	$10^{17}–10^{18e}$	$1.05×10^5$	η_1*	$10^{-13}–10^{-12}$
g	Gravity	m s^{-2}	9.8	9.8	$g*$	1
σ	Normal stress at the base of upper layer (lithostatic pressure$=\rho_u g h_u$)	Pa	$2.4×10^8$	480	$\sigma*$	$2×10^{-6}$

Values in round brackets relate to some experiments in which lower viscosity silicone has been used (trade name: SGR 36, produced by Dow Corning, UK), values in square brackets are for experiments with a brittle intrusion. Sources: (a) Metaxian (1994). (b) A minimum height for the silicone lower layer relative to the height of the upper brittle layer is necessary to represent the ductile crust (van Wyk de Vries and Merle, 1996), but silicone layer cannot be thicker than 2 cm because of edge effects. (c) For a crust composed of sedimentary rocks and tuffs (van Wyk de Vries, 1993). (d) Krantz (1991) and Schellart (2000) measured values of cohesion $>10^2$ Pa for sand. These values are open to debate and some authors sometimes consider no cohesion (e.g. Merle and Borgia, 1996). (e) Viscosity of the inner crust has to be $<3×10^{21}$ Pa s as for stiff sedimentary rocks (Gratier et al., 1999) but $>10^{18}$ Pa s as for melting granites (Wickham, 1987). Intrusion is hotter, thus less viscous. Origin of the other values is either measurements made in this study (viscosities were measured with a rotational viscometer) or values generally accepted in literature.

Table 2
Dimensionless numbers used to verify dynamic similarity, and the forces that characterize the system

Symbol	Definition	Expression	Value Nature	Models	Observation	Consequence
Π_5	$\dfrac{F_g}{F_\eta}$	$\rho_u g h_u \dfrac{t}{\eta_l}$	1^a	1^a	Equivalent in models and nature ($\Pi_5^* = 1$)	
Π_6	$\dfrac{F_r}{F_\eta}$	$\left[C_u + \left(\rho_u g h_u - \dfrac{\rho_u g h_u - 2 C_u \sqrt{3}}{3} + \dfrac{\eta_l}{t} \right) \tan\Phi \right] \dfrac{t}{\eta_l}$	$0.6\text{–}1.7^a$	$1\text{–}1.3^a$	Equivalent in models and nature ($\Pi_6^* \sim 1$)	
$\Pi_7 = Re$ (Reynolds number)	$\dfrac{F_i}{F_\eta}$	$\dfrac{\rho_l h_l^2}{\eta_l t}$	$10^{-23}\text{–}10^{-19a}$	$10^{-10}\text{–}10^{-8a}$	Different in models and nature, but much smaller than Π_5 and Π_6: inertia forces are negligible and $\Pi_7^* \sim 1$ is thus not required to respect dynamic similarity (Merle and Borgia, 1996)	Dynamic similarity
F_g	Gravity force	$\rho_u g h_u^b$				
$F_r(\tau)$	Failure resistance force	$C_u + (\sigma_1 - \sigma_3)\tan\Phi^b$ $\Leftrightarrow F_r = C_u + \left(\rho_u g h_u - \dfrac{\rho_u g h_u - 2 C_u \sqrt{3}}{3} + \dfrac{\eta_l}{t} \right) \tan\Phi$ with $\Phi = 30^{\circ b}$			Coulomb−Navier failure criterion with cohesion (Hubbert and Rubey, 1959)	
F_i	Inertia force	$\dfrac{\rho_l h_l^2}{t^2}^b$				
F_η	Viscous force	$\dfrac{\eta_l^b}{t}$				
σ_1	Maximal stress (lithostatic pressure)	$\rho_u g h_u$				
σ_3	Minimal stress	$\dfrac{\sigma_1 - a}{b} - \dfrac{\eta}{t}$				
a		$2 C_u b^{1/2}$				
b		$\dfrac{1 + \sin\Phi}{1 - \sin\Phi}$	3^c	3^c		

See Hubbert and Rubey (1959) and Merle and Borgia (1996) for details.

[a] By considering

$$t = \frac{\eta_l}{\rho_u g h_u}.$$

[b] Per area unit, Merle and Borgia (1996).

[c] With $\Phi = 30^\circ$ (Table 1).

Table 3
List of the experiments

Experiment no.	Description	Ductile lower layer	Intrusion	Topography	Strike-slip motion velocity mm h^{-1}	Additive extension (and opening velocity) (mm h^{-1})	Observation
S1	Static	Low-viscosity	Iron-sand	–	–	–	No subsidence
S2	Static, without scaling	Low-viscosity and density, 10 cm thick	Pure iron powder	–	–	–	Strong subsidence
S3	Static	1.5 cm thick	Iron-silicone	–	–	–	No subsidence
D212	No intrusion	1.5 cm thick	–	–	3.2	–	Pop-ups and Riedel shears
D213	As D212	1.5 cm thick	–	–	3.2	–	Dominating border effects
D215	Ductile intrusion	1.5 cm thick	Iron-silicone	–	5.4	–	Pull-apart above the intrusion+border effects
D219	Brittle intrusion	1.5 cm thick	Iron-sand	–	5.4	–	As D212
D220	Topography effect	1.5 cm thick	–	Volcano+ caldera	5.4	–	As D212 and no effect of topography
D221	As D215	1.5 cm thick	Iron-silicone	–	5.4	–	Thrusts above the intrusion
D222	As D219	1.5 cm thick	Iron-sand	–	5.4	–	As D219
D225	As D215/D221+topography	1.5 cm thick	Iron-silicone	Volcano+ caldera	5.4	–	As D221 and no effect of topography
D227	Additive extensive motion	1.5 cm thick	Iron-silicone	–	3.2	4° (0.22)	As D215
D228	Additive compressive motion	1.5 cm thick	Iron-silicone	–	3.2	−4° (−0.22)	Thrusts above the intrusion
D301	As D227, with reduced velocity	1.5 cm thick	Iron-silicone	–	1.6	4° (0.11)	Pull-apart above the intrusion without border effects
D305	As D301, with increased extension	1.5 cm thick	Iron-silicone	–	1.6	8° (0.22)	As D301
D306	As D301, with increased extension	1.5 cm thick	Iron-silicone	–	1.6	12° (0.33)	As D301
D308	Transtension	1.5 cm thick	–	–	3.2	8° (0.44)	Oblique rifts
D313	As D306	1.5 cm thick	Iron-silicone	–	1.6	12° (0.33)	As D301
D326	As D215, with reduced velocity and larger experimental setup for comparison	1.5 cm thick	Iron-silicone	–	1.6	–	Thrusts
D327	As D215, with reduced velocity	1.5 cm thick	Iron-silicone	–	1.6	–	Thrusts
D402	As D215, with low-viscous silicone layer	Low-viscosity and density, 2 cm thick	Iron-silicone	–	16 *	–	Thrusts
D403	As D215, with reduced velocity	1.5 cm thick	Iron-silicone	–	1.6	–	Thrusts
D418	As D402, with increased velocity	Low-viscosity and density, 2 cm thick	Iron-silicone	–	32*	–	Thrusts
D513	As D402, with increased velocity	Low-viscosity and density, 2 cm thick	Iron-silicone	–	54*	–	Thrusts
D514	As D215	1.5 cm thick	Iron-silicone	–	5.4	–	Thrusts
D515	As D215, with increased ductile layer thickness	Thicker (1.8 cm)	Iron-silicone	–	5.4	–	Pull-apart above the intrusion without border effects

The thickness of the silicone layer was chosen thinner than 2 cm (equivalent to a 6 km ductile layer). This is less than the value probable for a 10 km thick Nicaragua lower crust. Properly scaled thicker ductile layer control experiments were not exploitable due to edge effects that destroyed the model at greater than a few mm displacement. We lowered the thickness of the silicone to avoid these effects. We assured that the structures produced showed closely similar results to the few successful thick models. Because the results were similar, we believe that the models should be applicable to cases were the lower crust ductile layer is thicker than used here (5–6 km). Table 1 lists all the physical parameters defining the system both in models and nature, and their ratios.

The speed applied to the experiments is ruled by kinematic similarity (Merle and Vendeville, 1995). Given that our silicone is Newtonian,

$$\sigma = \frac{\eta_l}{t} \tag{1}$$

implying

$$\sigma^* = \frac{\eta_l^*}{t^*}. \tag{2}$$

Where σ=stress, η_l=viscosity of the ductile layer, and t=time. And

$$\sigma = \rho_u g h_u. \tag{3}$$

(Table 1; Merle and Vendeville, 1995), where ρ_u=density of rock, g=gravity and h_u=height (we use the standard crustal thickness for reference). This implies that:

$$\sigma^* = \rho_u^* g^* h_u^*. \tag{4}$$

So

$$t^* = \frac{\eta^*}{\rho_u^* g^* h_u^*} \tag{5}$$

And

$$t^* = \frac{x^*}{v^*} \tag{6}$$

with x and v displacement and velocity. So

$$v^* = \frac{\rho_u^* g^* h_u^{*2}}{\eta_l^*} \tag{7}$$

because $x^*=h_u^*$ owing to geometric similarity. t^* and v^* are about 10^{-10} and 10^3–10^4, respectively, so the velocity of strike-slip displacement to apply is about 1–10 mm/h, given that strike-slip displacement along the Nicaraguan Depression is 14 mm/year (DeMets, 2001).

A first approximation for dynamic similarity is respected if the ratio model/nature of cohesion and normal stress are equivalent (Merle and Borgia, 1996). This condition is fulfilled (Table 1). This also requires the ratios of the different forces being equivalent in models and nature. The forces, their expression, and their ratio are presented in Table 2. It appears that the force ratios defined as Π_5 and Π_6 have close values in models and nature. Thus dynamic similarity is also respected for forces.

5. Results

5.1. Preliminary experiments

We first tested the effect of an intrusive body without any tectonic motion. With correct scaling, no subsidence was observed at the surface even after 1 week (equivalent to 7 Ma in nature) (experiment S3, Table 3). Subsidence was only produced using a much denser intrusion, made of pure iron powder-ρ=3200 kg m^{-3}—and a silicone basal layer one order of magnitude less viscous than the silicone used in the other experiments (Table 3; experiment S2). The shape of the subsidence zone always strictly followed the shape of the intrusion. This

Notes to Table 3:
The added orthogonal component is expressed as an angle, the angle formed between the orientation of the basal moving sheet and the axis of displacement created by the motor. Negative value is for a compression component. The equivalent orthogonal displacement velocity, dependent on this angle and the lateral velocity of motion is also given. See Fig. 4 for details.
  * Velocity has to be increased of one order of magnitude, given that the silicone layer is one order of magnitude less viscous than in other experiments. See Table 1 and Section 4.2 for details and explanation.

mechanism is thus not reasonable for probable density contrasts of magmatic intrusions in the upper crust and upper crustal thicknesses. The reason for no deformation is linked to the presence of the upper brittle layer. This provides a resistance to sinking that is not overcome except with very dense intrusions on thicker and less dense silicone layer layers (Table 3; experiment S2).

We also ran control experiments with strike-slip tectonic motion, but without any intrusion (Table 3; D212). No pull-apart basin formed at the surface. We only observed pop-ups and Riedel shears. Even with transtensive tectonics (Table 3; D308), no pull-apart basin formed. By adding a component of extension to the motion, we only formed oblique rifts running through the entire model, but no pull-apart basins (Fig. 5A), as previously modeled by Tron and Brun (1991).

We also considered the effect of topography (Table 3; D220), assuming that the volcano would represent an overload and influence faulting, as described by van Wyk de Vries and Merle (1998). However, Las Sierras is made of low density pyroclastic products (van Wyk de Vries, 1993; Metaxian, 1994), and it is only 934 m a.s.l. for 30,000 m radius. Even by exaggerating the height of the volcano or by making a circular volcano and caldera (as it might have been before caldera-forming eruptions and erosion), we did not observe any effect of the volcano on strike-slip faulting (Fig. 5).

In the experiments only a modeled intrusive body is able to cause surface subsidence structures like those seen at Las Sierras-Masaya.

5.2. The effect of an intrusion coupled with strike-slip faulting

The Las Sierras intrusion is believed to be almost completely solid gabbro (Metaxian, 1994). However, there is still an active plumbing system and active degassing at Masaya Volcano (Rymer et al., 1998), and the Las Sierras Caldera is possibly only 30,000 years old (Bice, 1980). So, the intrusion is probably much hotter than the surrounding rocks and can be considered as slightly ductile, with a very high viscosity (Table 1). That is why most of the experiments were made with a ductile intrusion.

We first considered the case of a brittle solidified intrusion. Experiments with a brittle intrusion made of a sand-iron powder mixture (Table 3; D219, D222) did not show any subsidence of the surface localized above the intrusion, Riedel shears formed first and
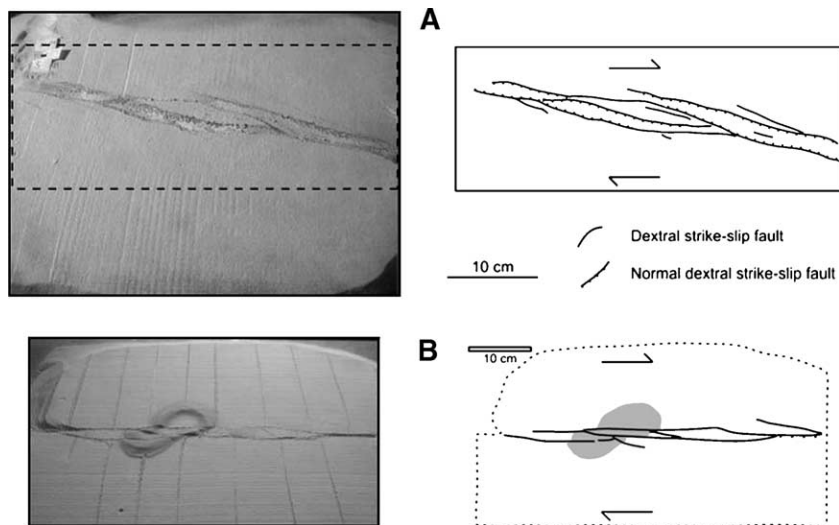

Fig. 5. (A) Experiment D308, with transtensive motion and no intrusion at an advanced stage (10 cm⇔30 km in nature, after 31 h⇔2 Ma). An oblique rift network formed but no pull-apart. This shows that transtension in a homogeneous crust is unable to create pull-aparts. (B) Experiment D220, with pure strike-slip motion, no intrusion and a volcanic shield representing Las Sierras-Masaya, at 7.2 cm⇔20 km in nature and after 13 h⇔850 ka. No fault deviation or pull-apart basin formed, showing that volcanic loading is also unlikely to create pull-aparts.
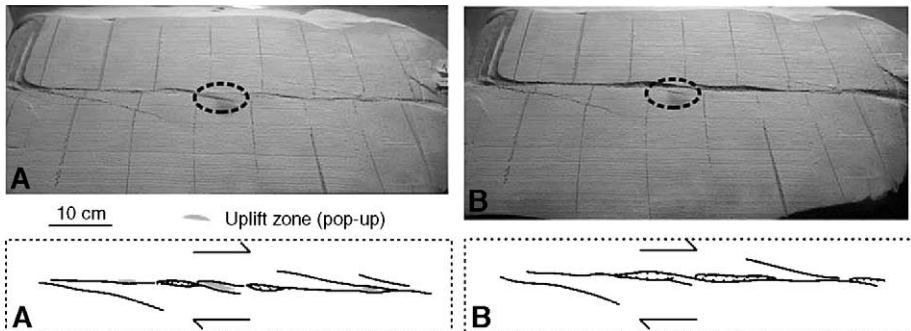
Fig. 6. Experiment D222, with pure strike-slip motion and a brittle and dense intrusion. The fault pattern above the intrusion evolves from a combination of small pop-ups and pull-aparts (A, displacement: 3.7 cm⇔10 km in nature, duration: 7 h⇔450 ka) to a longitudinal graben (B, displacement: 12 cm⇔35 km in nature, duration: 22.5 h⇔1.5 Ma). There is no fault deviation above the intrusion, suggesting that a dense but brittle intrusive body is not able to generate subsidence of a rhombic basin under the effect of the strike-slip motion. Dashed circles represent the location of the intrusion.

then, grabens (Fig. 6). The faults were not confined to the intrusion and showed no deflection as they passed through it. Thus the brittle intrusion had no effect on the overall pattern of deformation.

By contrast, with a ductile intrusion (Table 3; D215) made of a silicone-iron powder mixture, the effect of the intrusion was immediately visible. Rapidly, a typical pull-apart rhomb-shaped subsidence
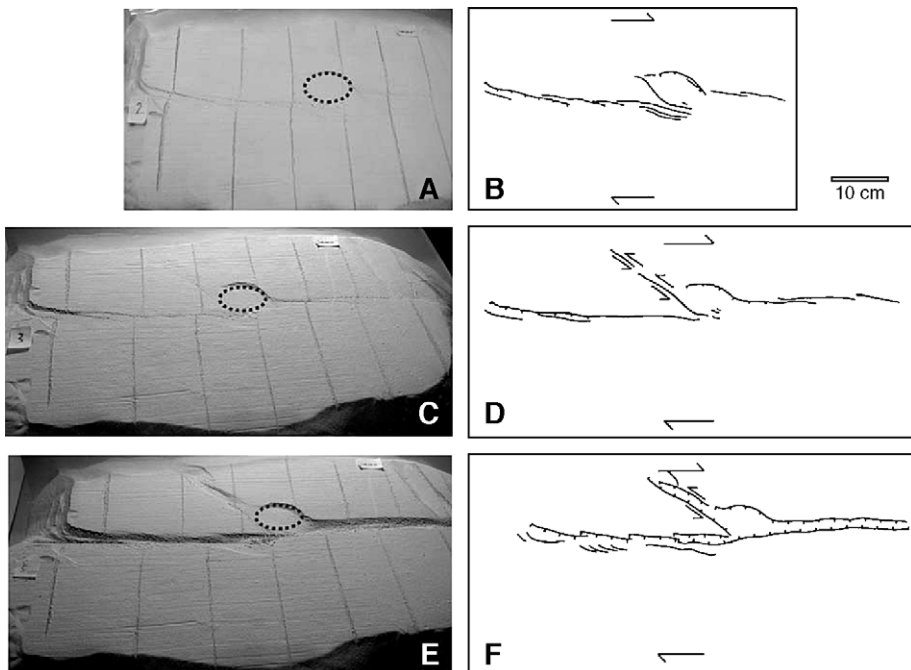

Fig. 7. Experiment D215, with pure strike-slip motion and a viscous and dense intrusion. First, a rhomb-shaped basin formed above the intrusion (A, B, displacement: 1.3 cm⇔4 km in nature, duration: 2.3 h⇔150 ka) while strike-slip faults were initiating from the corners of the subsiding rhomb-shaped basin to the edges of the model. Then, left-lateral faults formed between the basin and the edge of the model (C, D, displacement: 2 cm⇔6 km in nature, duration: 3.8 h⇔250 ka). Later, subsidence of the rhombic basin continues, the dextral strike-slip faults evolve into dextral normal strike-slip faults and the left-lateral faults evolve into a left-lateral graben that extend the rhombic basin (E, F, displacement: 6.5 cm⇔20 km in nature, duration: 12.5 h⇔800 ka), similar to the Managua Graben. Dashed circles represent the location of the intrusion.

zone formed, directly above the intrusion (Fig. 7). Once the pull-apart basin was formed, left-lateral transtensive conjugate faults formed in the moving part of the model, as an extension of the pull-apart basin (Fig. 7). We termed this feature lateral graben, as it extends laterally out from the pull-apart structure. The final shape and size of the subsidence zone (scaled up to nature), were strikingly similar to the Managua Graben and Las Sierras-Masaya volcanic complex.

The experiment D215 illustrates the capacity of a dense and viscous intrusive body to create a pull-apart basin under the effect of strike-slip tectonics. A repeat experiment (Table 3; D221) was made, especially to see if the lateral graben was an artifact. In this experiment the rhomb shape appeared, but instead of producing a pull-apart it created an uplift structure bounded by thrusts (Fig. 8). This experiment indicated that results were not easily reproducible. The main problem appeared to be that very small deviations from pure strike-slip motion were occurring. As indicated above in the experimental procedure the accuracy of the set up is about $\pm 1°$. It is clear that very small components of orthogonal movement have a large effect on the system. This phenomenon has also been observed when studying fault controlled destabilization of volcanic edifices (Lagmay et al., 2000; Wooller et al., 2003). When the system was constrained to transtension with more than $1°$ either side of pure strike-slip, pull-apart were consistently produced. When the system was constrained with more than $1°$ into transpression pup-up structures formed only.

The main questions (apart from reproducibility) raised by the repeat experiments were: (1) How could a pull-apart or reverse structure be formed? (2) How could the rhomb-shape be extended by a lateral graben?

5.3. Conditions for pull-apart/reverse structure formation

In the models the pull-apart structures have a classical form, while the uplifts are morphologically similar to the pressure ridges that are found along strike-slip faults (Aydin and Nur, 1982). A possible explanation for their formation is that a small degree of extension could have appeared in the first experiment, while a slight compression appeared in the second. This could be caused by a slight rotation of the basal sheet and the $1–2°$ error that exists in defining pure strike-slip in the apparatus. As mentioned above, such small initial rotations can cause major structural changes (Lagmay et al., 2000; Wooller et al., 2003).

We also checked if the rhomb-shaped subsidence/uplift effect were not a geometric effect, due to placing the intrusion at the center of the model. The intrusion was offset and the uplift, or pull-apart still occurred above it.

The effect of transpression/transtension was verified by experiments with transtensive and a transpressive motion (Table 3; D227 and D228). Transtension formed a pull-apart subsidence zone, while transpression formed a rhomb-shaped uplift zone bounded by symmetrical thrusts (Fig. 8). Experiments with greater extension (angle of $8°$, experiment D305, angle of $12°$, experiments D306 and D313) also showed a rhomb-shaped graben above the intrusion. Thus, transtension is necessary to generate a pull apart at the intrusion; otherwise a compressive pop-up structure is produced. It is clear from the experiments with near strike-slip motion that $1°$ or less of orthogonal component is enough to switch from pull-apart to pup-up structure.

5.4. Conditions of formation of lateral Graben

During the running of the initial experiment (D215), the lateral graben rapidly reached the model corner (Fig. 7), which could indicate a controlling border effect, even if the deformation rate was at the mid range of our permitted scaling. There is a crustal change at the Nicaraguan Depression northeast boundary, between thin ophiolitic crust and continental granitic crust of the Chortís Blocks (Weinberg, 1992; van Wyk de Vries and Borgia, 1996). The model set up therefore may represent this very particular case, applicable to Nicaragua, where the deformation is perturbed by a local boundary effect.

We tested the effect of deformation rate on the lateral graben formation. We observed that a speed change from 5.4 mm/h (D215) to 3.2 mm/h (D227) had no influence on the formation of this structure. However, at even slower rates (experiment D301: 1.6 mm/h) the lateral graben did not form (Fig. 9). Repeat
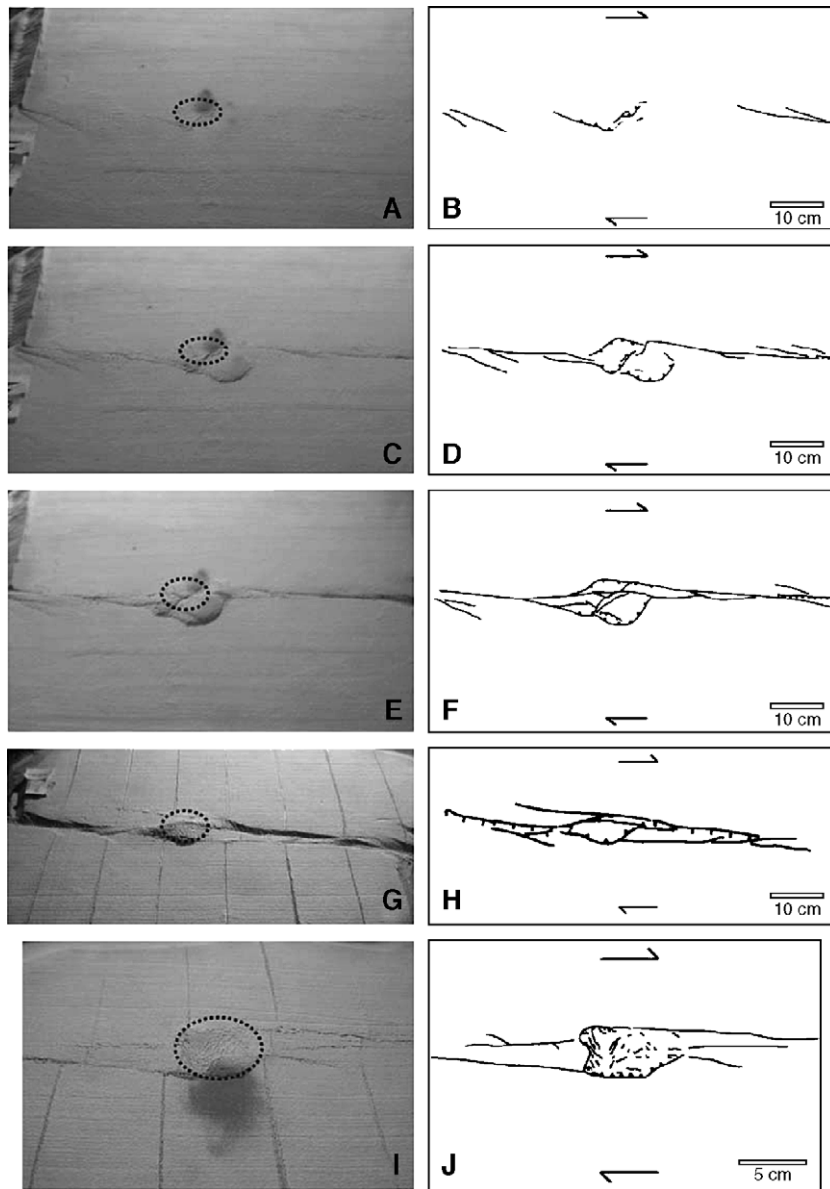
Fig. 8. Examples of thrusts that formed above the intrusion during some experiments. In many experiments such as D326–the one that provided the most typical results–the first structures observed are thrusts (A, B, displacement: 2.1 cm⇔6 km in nature, duration: 13 h⇔850 ka) instead of the subsidence observed in D215. Then, the uplift zone becomes symmetrical and rhombic and is joined in its extremities by the major strike-slip faults created by the strike-slip motion (C, D, displacement: 3.6 cm⇔10 km in nature, duration: 22.75 h⇔1.5 Ma). It describes a pressure ridge (Aydin and Nur, 1982). The uplift zone is depressed at its center and deviates the main strike-slip fault (C, D). But this is still uplift relative to the original elevation of the model. Later, the uplift zone became inactive and waned, cut directly by the main strike-slip faults (E, F, displacement: 6.1 cm⇔17.5 km in nature, duration: 38 h⇔2.5 Ma). The fault pattern inside the uplift zone was very variable from one experiment to another, without any depression and deviation of the main strike-slip faults (G, H, experiment D221, displacement: 10.5 cm⇔30 km in nature, duration: 19.5 h⇔1.25 Ma), or with very complex fault patterns probably resulting from folding (I, J, experiment D228, displacement: 3.6 cm⇔10 km in nature, duration: 11.25 h⇔750 ka). Nevertheless a common point between all the uplift structures formed is their rhombic shape, as it is the case for the experiments forming subsidence basins. Dashed circles represent the location of the intrusion.
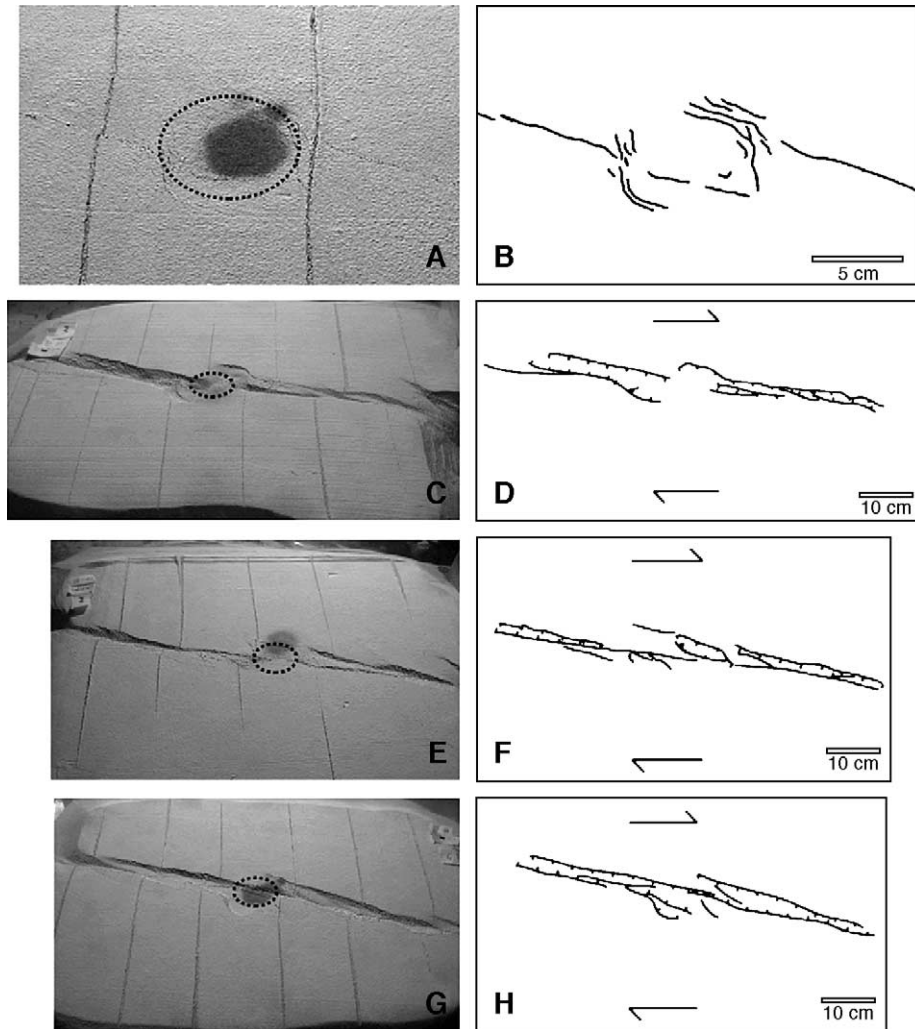
Fig. 9. Examples of pull-aparts that formed during experiments with transtension. (A) and (B) represent the first faults observed in experiment D306 (transtensive motion of 12°⇔0.33 mm/h of opening and 1.6 mm/h of strike-slip displacement, displacement: 1.0 cm⇔3 km in nature, duration: 6 h⇔400 ka). A rhombic basin along juvenile strike-faults is clearly visible. It forms above the intrusion (of circular section) like in all the other experiments. At more evolved stages, at higher displacement rates, the pull-apart basin is still subsiding and the juvenile strike-slip faults evolve in oblique rifts, whatever the extensive component: C, D, experiment D301 (transtensive motion of 4°⇔0.11 mm/h of opening and 1.6 mm/h of strike-slip displacement, displacement: 5.6 cm⇔16 km in nature, duration: 35.25 h⇔2.3 Ma); E, F, experiment D305 (transtensive motion of 8°⇔0.22 mm/h of opening and 1.6 mm/h of strike-slip displacement, displacement: 4.3 cm⇔12 km in nature, duration: 27 h⇔1.75 Ma); G, H, experiment D306 (transtensive motion of 12°⇔0.33 mm/h of opening and 1.6 mm/h of strike-slip displacement, displacement: 3.8 cm⇔11 km in nature, duration: 23.5 h⇔1.5 Ma). Dashed circles represent the location of the intrusion.

experiments were also run at this slow rate with increasing extension component (Table 3; D305, D306 and D313) and no lateral graben formed (Fig. 9). Two experiments with near strike-slip motion were also run at that velocity (D327 and D403): no lateral structure formed, but only an uplift zone with thrusts.

From these results the lateral graben can be interpreted as resulting from an instability that occurs in the model at moderate—high deformation rates under small amounts of transtension. The instability may be caused by either strain build up at the interface between the cohesive brittle sand

layer and the silicone, or a strain rate related stiffening of the silicone. As the rate of motion in all experiments is very slow and the strain rate changes by just a small amount, we suggest that the strain rate build up at the interface may be dominantly responsible. Both processes strain rate related effect and viscous—brittle boundary effects will occur in nature.

Interestingly for this study, the Managua Graben has a pull-apart basin shape extended by a lateral graben and thus the specific formation conditions of the feature in the model may be applicable to Las Sierras-Masaya.

5.5. Role of density

We tested the role of density contrasts using experiments with increased and decreased density contrast between the intrusion and its ductile substratum. Whatever the density contrast, subsidence did not occur, but uplift did (experiments D402, D418, D513 with a silicone substratum 530 kg/m^3 less dense than the intrusion, instead of 60 kg/m^3 less dense in the other experiments). This observation is in accordance with the results of experiments D219 and D222 with brittle and denser intrusion of 2000 kg/m^3 (hence a substratum 450 kg/m^3 less dense than the intrusion) that did not produce subsidence and suggests that density could not be a controlling factor in creating subsidence.

5.6. Summary

Experiments show that pull-apart basin formation around large volcanic complexes in context of strike-slip tectonics can be a consequence of the presence of the underlying ductile intrusion. To generate a pull-apart basin in this context, both transtensional strike-slip motion and a ductile intrusion are required. Experiments without tectonic motion do not produce rhomb features, not surprisingly. However, strike-slip motion, even transtension, does not produce pull-aparts with no intrusion. A shield-like volcanic overload has no effect either. A brittle intrusion cannot generate a pull-apart basin above it, even if very dense. The intrusion must be ductile. Last, density contrasts have no detectable influence on the results.

Experiments with small amounts of transtension and a ductile intrusion form pull-apart basins above a circular intrusion (Fig. 7 and Fig. 9). However uplift zones can appear instead in transpression (Fig. 8). An important detail is that the structure is always rhomb-shaped, while the intrusion in our models is always circular.

The rate of strike-slip motion does not control the type of structure that forms, but at the highest reasonable displacement rates (equal to 4.7 mm per year) there are instabilities in the model and boundary effects can appear, generating an asymmetric pull-apart basin extended by a graben, similar to the Managua Graben (Fig. 7).

6. Discussion

6.1. Origin of the Managua Graben

This series of experiments provides numerous results. First, the only way we have found to create a pull-apart basin such as the Managua Graben is to associate a ductile intrusive complex and transtension. Indeed, experiments without intrusion (even in transtension) did not produce pull-apart basins (Table 3). We propose that the underlying magmatic complex is responsible for; (1) the location of pull-apart structure and (2) the opening of the Managua Graben, given that it is placed in the regional strike-slip tectonic motion that characterizes the Nicaraguan Depression. We note that a slight additional extensive motion is required for the pull-apart basins to form in this context. This extension exists in the Nicaraguan depression as a result of Chortís Block rotation (Cruden, 1988; Weinberg, 1992; van Wyk de Vries, 1993).

The Managua Graben does not have the typical rhombic shape of pull-apart basins: it is extended northward by two normal sinistral faults (Cofradías and Punta Huete Faults) that define a graben (Fig. 3) and reach the northeastern edge of the Nicaraguan Depression. They may also continue northward in the Nicaraguan Highlands. Indeed, some extensional structures have been mapped in this area. The Sebaco graben, for instance is located exactly north Managua Graben (van Wyk de Vries, 1993), and the Chortís block is cut by several old north- and northeast-

orientated faults such as Guayape fault (Fig. 1) (Gordon and Muehlberger, 1994). It is possible that two north-striking ancient faults were reactivated during the Pleistocene, while the Managua Graben was opening. In addition, the models show a pre-disposition to form such geometry. So the unusual shape of the Managua Graben is probably the consequence of the interaction between the volcano-tectonic pull-apart pre-disposed to asymmetry and possibly inherited faults.

6.2. Generalization: natural pull-aparts and caldera complexes

The experiments were run to specifically model the Nicaraguan situation, but they can be generalized. Many large volcanic complexes and associated intrusions are present along strike-slip fault zones, and we note a close association between pull-apart basins and large volcanic systems with large calderas. For example Deception Island, Antarctica may be a pull-apart related caldera. (Martí et al., 1996). Amatitlàn Caldera, Guatemala, is also a caldera lying along a strike-slip fault, Jalpatagua Fault (Fig. 1). Its eastern and western bounding faults coincide with the Guatemala City Graben, a graben perpendicular to Jalpatagua Fault (Wunderman and Rose, 1984). Numerous striking examples exist along the Great Sumatran Fault Zone, one of the fastest strike-slip zones in the world. Many volcanic complexes lie along the fault, such as Suwoh, Ranau and Toba calderas. They have long been considered as volcano-tectonic depressions (van Bemmelen, 1949).

Toba Caldera is thought to have developed first as a pull-apart basin. Then an intrusive-volcanic system developed. Lastly, several ignimbrite caldera-forming eruptions occurred, and caldera collapses finally followed the boundaries of the pull-apart (Detourbet et al., 1993). Suwoh and Ranau Calderas lie in active pull-apart basins as well, (Bellier and Sébrier, 1994). Ranau Caldera has partially collapsed along the pull-apart sides. Suwoh by contrast has not and Bellier and Sébrier (1994) suggest that Suwoh is a system comparable to Ranau or Toba, but that collapse into the intrusion has not yet involved the marginal faults.

The same pull-apart model can be used to explain the polygonal shape of Tondano Caldera, on Sulawesi Island, Indonesia, also located along a strike-slip zone. Evidence of a pre-caldera pull-apart basin has also been found (Lécuyer et al., 1997).

In the Central Volcanic Zone of the Andes (Bolivia/Chile/Argentina), many Tertiary calderas, now active resurgent domes, lie along the sinistral strike-slip Calama-Olacapato-El Toro and Archibarca faults (Matteini et al., 2002). The Aguas Calientes Caldera (Matteini et al., 2002), Cerro Galan Caldera (de Silva and Francis, 1991) and La Pacana Caldera (de Silva and Francis, 1991; Lindsay et al., 2001) also show evidence of subsidence along normal tectonic faults mostly perpendicular to the strike-slip faults. This is particularly marked along the Aguas Calientes Caldera (de Silva and Francis, 1991). These faults could have delimited former pull-apart basins or rhombic grabens similar to the Indonesian systems.

The 630 ka old Yellowstone Caldera, Wyoming, USA might have been emplaced in similar strike-skip conditions: it is elongated (Christiansen, 2001) and lies at the boundary of the extensional Basin and Range Province at South, and the Northern Rocky Mountains at North, where extension is much less developed. This results in a strike-slip tectonic regime (Hooper et al., 2002) for which no clear strike-slip fault is identifiable, similar to the Nicaragua Depression. The caldera is viewed as elliptical by Christiansen (2001) but its boundaries, extensively buried by more recent lava flows are not well constrained and may instead follow regional NNW- and NW-trending normal faults, defining a more rectangular caldera instead.

Interestingly, its underlying intrusive magmatic system does not follow the caldera boundaries but is rather made of two smaller magma intrusions (Miller and Smith, 1999; Husen et al., 2004). Similar observations have been made for Toba (Masturyono et al., 2001). This is in good accordance with our models, in which the faulting pattern formed at the surface does not have the shape of the intrusion.

The presence of pre-existing faults is one possible cause of pull-aparts (Lécuyer et al., 1997), though this has not been tested experimentally. The Managua Graben, as well as Tondano Caldera and Yellowstone Caldera, could be the result of an interaction between both phenomena.

Intrusion related density contrasts do not appear to be controlling factors, as experiments performed with

exaggerated density contrasts did not show more significant subsidence. In addition Amatitlàn, Yellowstone, the Indonesian and Andean systems are silicic, which means that the magmatic chambers were not necessarily much denser than the surrounding rocks like at Las Sierras-Masaya.

6.3. Generalization: natural-pop-up structures related to intrusions

The experiments showed that rhomb-shaped uplift zones bounded by thrusts can form above intrusions. Examples of volcanic complexes bounded by thrusts are much less common than ones bounded by pull-apart basins. In general the same is true for pressure ridges relative to pull-apart basins in non-volcanic settings (Aydin and Nur, 1982). Possible examples are the Cerro de Coransoque and Cordon Puntas Negras Tertiary volcanic complexes (Atacama Desert, N Chile/Argentina). These are cut by strike-slip faults (Matteini et al., 2002) and are bordered on one side by thrust zones (van Wyk de Vries et al., 1996).

Magmatic complexes usually do not keep a constant volume as they erupt and originate caldera subsidence, whereas intrusions in the experiments kept a constant volume without erupting. The emptying of magmatic chambers and caldera formation are probably likely to enhance formation of subsidence zones instead of uplift zones.

7. Conclusions

A morpho-structural analysis has showed that the Managua Graben strictly encloses Las Sierras-Masaya volcanic complex and is a modified rhomb-shape with a northern extension. Its location in a strike-slip zone (the Nicaraguan Depression) allows us to consider it as a pull-apart basin. Our analogue experiments show that in transtension, a ductile intrusion can localize deformation and generate a pull-apart. We suggest that the Managua Graben has developed as a consequence of the weak magmatic intrusion under Las Sierras-Masaya Caldera. More generally, intrusions associated with large volcanic complexes may initiate pull-apart basin formation along strike-slip fault zones. Striking similarity between Las Sierras-Masaya and Suwoh Caldera is observed, and the long-term model of

evolution proposed by Bellier and Sébrier (1994) for Suwoh may reasonably be applied to Las Sierras-Masaya. That would correspond to a partial collapse of the Managua Graben (a densely populated area hosting Managua City) if a great eruption did occur. However the basaltic nature of the magma involved at Masaya and the limitation of the active system to the Masaya Caldera could be a limiting factor for such a long-term evolution. Nevertheless, given that there is a probable genetic link between the Managua Graben and Las Sierras-Masaya volcanic complex (Brown et al., 1973; Rymer et al., 1998) a joint monitoring of volcano and graben is appropriate.

References

Aydin, A., Nur, A., 1982. Evolution of pull-apart basins and their scale independence. Tectonics 1, 91–105.

Bellier, O., Sébrier, M., 1994. Relationship between tectonism and volcanism along the Great Sumatran Fault Zone deduced by SPOT images. Tectonophysics 233, 215–231.

Bice, D.C., 1980. Tephra stratigraphy and physical aspects of recent volcanism near Managua, Nicaragua. PhD Thesis, Univ. of California, Berkeley, CA, USA.

Branquet, Y., van Wyk de Vries, B., 2001. Effets de la charge des édifices volcaniques sur la propagation de structures régionales compressives: exemples naturels et modèles expérimentaux. C. R. Acad. Sci. Paris, Sci. Terre Planètes 333, 455–461.

Brown Jr., R.D., Ward, P.L., Plafker, G., 1973. Geologic and seismologic aspects of the Managua, Nicaragua, earthquakes of December 23, 1972. Geol. Surv. Prof. Pap. 838. 34 pp.

Burkart, B., Self, S., 1985. Extension and rotation of crustal blocks in northern Central America and effect on the volcanic arc. Geology 13, 22–26.

Burton, M.R., Oppenheimer, C., Horrocks, L.A., Francis, P.W., 2000. Remote sensing of CO (sub 2) and H (sub 2) O emission rates from Masaya Volcano, Nicaragua. Geology 28, 915–918.

Christiansen, R.L., 2001. The Quaternary and Pliocene Yellowstone Plateau volcanic field of Wyoming, Idaho and Montana. U. S. Geol. Surv. Prof. Pap. 729-G. 145 pp.

Cobbold, P.R., Castro, L., 1999. Fluid pressure and effective stress in sandbox models. Tectonophysics 301, 1–19.

Connor, C.B., Williams, S.N., 1989. Interpretation of gravity anomalies, Masaya Caldera complex, Nicaragua. Preprint: Transaction of the 12th Caribbean Conference, St Croix, Virgin Islands.

Cruden, A.R., 1988. The structure of South-western Nicaragua: a preliminary assessment. Rep. URAP 89001, Swed. Agency for Res. Coop. with Dev. Countries, Inst. Nicaragüense de Mineria, Swedish Geological A.B., Luleå, Sweden.

Cyr, K.E., Melosh, H.J., 1993. Tectonic patterns and regional stresses near Venusian coronae. Icarus 102, 175–184.

Delmelle, P., Stix, J., Baxter, P.J., Garcia-Alvarez, J., Barquero, J., 2002. Atmospheric dispersion, environmental effects and potential health hazard associated with the low-altitude gas plume of Masaya Volcano, Nicaragua. Bull. Volcanol. 64, 423–434.

DeMets, C., 2001. A new estimate for the present-day Cocos-Carribean plate motion: implications for slip along the Central American volcanic arc. Geophys. Res. Lett. 28, 4043–4046.

de Silva, S.L., Francis, P.W., 1991. Volcanoes of the Central Andes. Springer-Verlag, Berlin, pp. 160–176.

Detourbet, C., Bellier, O., Sébrier, M., 1993. La caldeira volcanique de Toba et la Grande Faille de Sumatra (Indonésie) vues par l'imagerie SPOT. C. R. Acad. Sci. Paris, Sér. II 316, 1439–1445.

Freund, R., 1974. Kinematics of transform and transcurrent faults. Tectonophysics 21, 93–134.

Glazner, F.A., Miller, D.M., 1997. Late-stage sinking of plutons. Geology 25, 1099–1102.

Gordon, M.B., Muehlberger, W.R., 1994. Rotation of the Chortís block causes dextral slip on the Guayape fault. Tectonics 13, 858–872.

Gratier, J.-P., Renard, F., Labaume, P., 1999. How pressure solution creep and fracturing processes interact in the upper crust to make it behave in both a brittle and viscous manner. J. Struct. Geol. 21, 1189–1197.

Hooper, P., Johnson, J., Hawkesworth, C., 2002. A model for the origin of the Western Snake River Plain as an extensional strike-slip duplex, Idaho and Oregon. In: Bonnichsen, B., White, C.M., McCurry, M. (Eds.), Tectonic and Magmatic Evolution of the Snake River Plain Volcanic Province, Idaho Geol. Surv. Bull., vol. 30, pp. 59–67.

Horrocks, L.A., Burton, M.R., Francis, P.W., Oppenheimer, C., 1999. Stable gas plume composition measured by OP-FTIR spectroscopy at Masaya Volcano, Nicaragua, 1998–1999. Geophys. Res. Lett. 26, 3497–3500.

Hubbert, M.K., Rubey, W.W., 1959. Role of fluid pressure in mechanics of overthrust faulting, I. Mechanisms of fluid-filled porous solids and its application to overthrust faulting. Geol. Soc. Amer. Bull. 70, 115–166.

Husen, S., Smith, R.B., Waite, G.P., 2004. Evidence for gas and magmatic sources beneath the Yellowstone volcanic field from seismic tomographic imaging. J. Volcanol. Geotherm. Res. 131, 397–410.

Krantz, R.W., 1991. Measurements of friction coefficients and cohesion for faulting and fault reactivation in laboratory models using sand and sand mixtures. Tectonophysics 188, 203–207.

La Femina, P.C., Dixon, T.H., Strauch, W., 2002. Bookshelf faulting in Nicaragua. Geology 30, 751–754.

Lagmay, A.M.F., van Wyk de Vries, B., Kerle, N., Pyle, D.M., 2000. Volcano instability induced by strike-slip faulting. Bull. Volcanol. 62, 331–346.

Lavallée, Y., Stix, J., Kennedy, B., Richer, M., Longpré, M.-A., 2004. Caldera subsidence in areas of variable topographic relief: results from analogue modeling. J. Volcanol. Geotherm. Res. 129, 219–236.

Lécuyer, F., Bellier, O., Gourgaud, A., Vincent, P.M., 1997. Tectonique active du Nord-Est de Sulawesi (Indonésie) et contrôle structural de la caldeira de Tondano. C. R. Acad. Sci. Paris, Sci. Terre Planètes 325, 607–613.

Lindsay, J.M., de Silva, S., Trumbull, R., Emmermann, R., Wemmer, K., 2001. La Pacana caldera, N. Chile: a re-evaluation of the stratigraphy and volcanology of one of the world's largest resurgent calderas. J. Volcanol. Geotherm. Res. 106, 145–173.

Manton, W.I., 1987. Tectonic interpretation of the morphology of Honduras. Tectonics 6, 633–651.

Martí, J., Vila, J., Rey, J., 1996. Deception Island (Bransfield Strait, Antarctica): an example of a volcanic caldera developed by extensional tectonics. In: McGuire, W.J., Jones, A.P., Neuberg, J. (Eds.), Volcano Instability on the Earth and Other Planets, Geol. Soc. Spec. Publ., vol. 110, pp. 253–265.

Masturyono, McCaffrey, R., Wark, D.A., Roecker, S.W., Fauzi, Ibrahim, G., Sukhar, 2001. Distribution of magma beneath the Toba caldera complex, north Sumatra, Indonesia, constrained by three-dimensional P wave velocities, seismicity, and gravity data. Geochem. Geophys. Geosyst. 2 (2000GC000096). 24 pp.

Matteini, M., Mazzuoli, R., Omarini, R., Cas, R., Maas, R., 2002. The geochemical variations of the upper cenozoic volcanism along the Calama-Olacapato-El Toro transversal fault system in central Andes (24°S): petrogenetic and geodynamic implications. Tectonophysics 345, 211–227.

McBirney, A.R., 1956. The Nicaraguan volcano Masaya and its caldera. Trans.-Am. Geophys. Union 37, 83–96.

McBirney, A.R., Williams, H., 1964. The origin of the Nicaraguan Depression. Bull. Volcanol. 27, 63.

McBirney, A.R., Williams, H., 1965. Volcanic History of Nicaragua. University of California Press, Berkeley, CA, USA.

McClay, K., Dooley, T., 1995. Analogue models of pull-apart basins. Geology 23, 711–714.

Merle, O., Borgia, A., 1996. Scaled experiments of volcanic spreading. J. Geophys. Res. 101, 13805–13817.

Merle, O., Vendeville, B., 1995. Experimental modelling of thin-skinned shortening around magmatic intrusions. Bull. Volcanol. 57, 33–43.

Metaxian, J.-P., 1994. Etude sismologique d'un volcan actif: dynamisme interne et structure de la caldeira Masaya, Nicaragua. PhD Thesis, Univ. de Savoie, Chambéry, France.

Miller, D.S., Smith, R.B., 1999. P and S velocity structure of the Yellowstone volcanic field from local earthquake and controlled source tomography. J. Geophys. Res. 106, 15105–15121.

Rymer, H., van Wyk de Vries, B., Stix, J., Williams-Jones, G., 1998. Pit crater structure and processes governing persistent activity at Masaya volcano, Nicaragua. Bull. Volcanol. 59, 345–355.

Schellart, W.P., 2000. Shear test results for cohesion and friction coefficients for different granular materials: scaling implica-

tions for their usage in analogue modelling. Tectonophysics 324, 1–16.

Šebesta, J., 1997. Dynamic development of the relief in the Managua area, Nicaragua. Acta Univ. Carol., Geogr. 2, 93–109.

Tron, V., Brun, J.-P., 1991. Experiments on oblique rifting in brittle-ductile systems. Tectonophysics 188, 71–84.

van Bemmelen, R.W., 1949. The Geology of Indonesia, General Geology of Indonesia and Adjacent Archipelagos. Government Printing Office, The Hague, Netherlands.

van Wyk de Vries, B., 1993. Tectonics and magma evolution of Nicaraguan volcanic systems. PhD Thesis, Open University, Milton Keynes, UK.

van Wyk de Vries, B., Borgia, A., 1996. The role of basement in volcano deformation. In: McGuire, W.J., Jones, A.P., Neuberg, J. (Eds.), Volcano Instability on the Earth and Other Planets, Geol. Soc. Spec. Publ., vol. 110, pp. 95–110.

van Wyk de Vries, B., Merle, O., 1996. The effect of volcanic constructs on rift fault patterns. Geology 24, 643–646.

van Wyk de Vries, B., Merle, O., 1998. Extension induced by volcanic loading in regional strike-slip zones. Geology 26, 983–986.

van Wyk de Vries, B., Self, S., Francis, P.W., 1996. Thin skinned thrusting caused by volcanism in N. Chile. Tectonic Studies Group, Research in Progress, Birmingham, UK, 12–16th December.

Walker, J.A., 1984. Volcanic rocks from the Nejapa and Granada cinder cone alignments, Nicaragua, Central America. J. Petrol. 25, 299–342.

Walker, G.P.L., 1988. Three Hawaiian calderas: an origin through loading by shallow intrusions? J. Geophys. Res. 93, 14773–14784.

Watters, T.R., Janes, D.M., 1995. Coronae on Venus and Mars: implications for similar patterns on Earth. Geology 23, 200–204.

Weinberg, R.F., 1992. Neotectonic development of Western Nicaragua. Tectonics 11, 1010–1017.

Wickham, S.M., 1987. The segregation and emplacement of granitic magmas. J. Geol. Soc. (Lond.) 144, 281–297.

Williams, S.N., 1983. Geology and eruptive mechanisms of Masaya caldera complex, Nicaragua. PhD Thesis, Dartmouth College, Hanover, NH, USA.

Wooller, L., Murray, J.B., Rymer, H., van Wyk de Vries, B., 2003. Volcano Instability and collapse from basement faulting. Geophys. Res. Abstr. 5, 00304.

Wunderman, R.L., Rose, W.I., 1984. Amatitlán, an actively resurging cauldron 10 km south of Guatemala City. J. Geophys. Res. 89, 8525–8539.